A widespread family of bacterial cell wall assembly proteins

The EMBO Journal (2011) 30, 4931–4941 | © 2011 European Molecular Biology Organization | All Rights Reserved 0261-4189/11
www.embojournal.org

THE EMBO JOURNAL

A widespread family of bacterial cell wall assembly proteins

Yoshikazu Kawai[1], Jon Marles-Wright[1], Robert M Cleverley[1], Robyn Emmins[1], Shu Ishikawa[2], Masayoshi Kuwano[2], Nadja Heinz[1], Nhat Khai Bui[1], Christopher N Hoyland[1], Naotake Ogasawara[2], Richard J Lewis[1], Waldemar Vollmer[1], Richard A Daniel[1] and Jeff Errington[1,*]

[1]Centre for Bacterial Cell Biology, Medical School, Newcastle University, Newcastle upon Tyne, UK and [2]Graduate School of Information Science, Nara Institute of Science and Technology, Nara, Japan

Teichoic acids and acidic capsular polysaccharides are major anionic cell wall polymers (APs) in many bacteria, with various critical cell functions, including maintenance of cell shape and structural integrity, charge and cation homeostasis, and multiple aspects of pathogenesis. We have identified the widespread LytR–Cps2A–Psr (LCP) protein family, of previously unknown function, as novel enzymes required for AP synthesis. Structural and biochemical analysis of several LCP proteins suggest that they carry out the final step of transferring APs from their lipid-linked precursor to cell wall peptidoglycan (PG). In *Bacillus subtilis*, LCP proteins are found in association with the MreB cytoskeleton, suggesting that MreB proteins coordinate the insertion of the major polymers, PG and AP, into the cell wall.

The EMBO Journal (2011) **30,** 4931–4941. doi:10.1038/emboj.2011.358; Published online 30 September 2011
Subject Categories: cell & tissue architecture; microbiology & pathogens
Keywords: capsular polysaccharide; LytR–CpsA–Psr proteins; MreB; peptidoglycan; teichoic acids

Introduction

The cell wall is crucial for maintaining the structural integrity and the characteristic shape of a bacterial cell. In Gram-positive bacteria, a group that contains many important pathogens, the cell wall has two major components: (i) peptidoglycan (PG), whose pathway is the target for some of our most successful antibacterial compounds (the β-lactams and glycopeptides) and (ii) the PG-attached anionic cell wall polymers (APs), including wall teichoic acids (WTAs) and acidic polysaccharides.

WTAs and their lipid-linked versions (lipoteichoic acids) have a wide range of important cellular roles including control of autolytic activity, antigenicity and innate immune recognition, pathogenicity, biofilm formation, efficient release of secreted proteins into the culture medium, cation homoeostasis, antibiotic resistance, and cell elongation and division (summarized in Weidenmaier and Peschel, 2008).

In *Bacillus subtilis*, WTA is present in large quantities, roughly equal to those of PG (Foster and Popham, 2002). Most steps in the synthesis of WTA are now known, catalysed by a variety of gene products with a *tag* prefix (Neuhaus and Baddiley, 2003; Brown *et al*, 2008). The polymer is synthesized in the cytoplasm, translocated across the membrane by the ABC transporter TagGH (Schirner *et al*, 2011), and is covalently attached to PG outside the cell (Yokoyama *et al*, 1989). The physical connection of major APs like WTA or capsular polysaccharides to PG builds the final cell wall architecture and is essential for proper cell wall functionality, but the enzyme catalysing this important step remains to be identified.

Disruption of most of the *tag* genes of *B. subtilis* is lethal. This lethality can be suppressed by deleting *tagO* or *tagA* to block the earliest steps in the pathway, which presumably prevents either the build up of a toxic intermediate or the sequestration of an essential metabolite. Nevertheless, *tagO* and *tagA* mutants are severely compromised in cell growth and they lose the ability to elongate, becoming rounded and swollen (D'Elia *et al*, 2006a, b, 2009). *tagO* null mutants of the round *Staphyloccocus aureus* have no significant growth defect but they are affected in spatial control of PG synthesis, are hypersensitive to lysozyme, and are badly impaired in virulence (Weidenmaier and Peschel, 2008; Atilano *et al*, 2010).

In most rod-shaped bacteria, cell elongation is governed largely by the prokaryotic actin homologue, MreB, which assembles into patches or filaments at the inner surface of the membrane (Graumann, 2009). MreB is essential for viability in many bacteria, and its depletion induces severe morphological defects (Jones *et al*, 2001; Figge *et al*, 2004; Kruse *et al*, 2005; Slovak *et al*, 2005; Hu *et al*, 2007). Many Gram-positive bacteria have more than one MreB isoform. The *B. subtilis* MreB isoforms, MreB, Mbl, and MreBH largely colocalize and have partially overlapping functions (Carballido-Lopez *et al*, 2006; Kawai *et al*, 2009a). MreB and Mbl are essential under normal growth conditions, although the mutants are viable in high Mg^{2+} concentrations for reasons that are not yet clear (Formstone and Errington, 2005; Schirner and Errington, 2009). Evidence from several laboratories supports the idea that the MreB cytoskeleton somehow spatially regulates the synthesis of PG and potentially other cell wall components, thereby bringing about controlled expansion of the wall, while retaining a defined cell shape (Daniel and Errington, 2003; Vats *et al*, 2009; Kawai *et al*, 2009b).

We have now obtained several lines of evidence supporting the idea of a direct role for the MreB cytoskeleton in WTA synthesis and cell wall attachment. By searching for MreB-interacting proteins, we have identified a widely distri-

*Corresponding author. Centre for Bacterial Cell Biology, Medical School, Newcastle University, Richardson Road, Newcastle upon Tyne NE2 4AX, UK. Tel.: +44 191 222 8126; Fax: +44 191 222 7424; E-mail: jeff.errington@ncl.ac.uk

Received: 9 August 2011; accepted: 31 August 2011; published online: 30 September 2011

buted family of proteins of previously unknown function, the LytR–Cps2A–Psr (LCP) family, as having a role in the biogenesis of WTA and anionic polysaccharides (Hübscher *et al*, 2008). LCP proteins are present in virtually all gram-positive bacteria, which characteristically contain PG-attached WTA and/or APs. Our structural and biochemical data on several LCP proteins provide strong evidence that this family of proteins carry out the key step of attaching APs to the cell wall PG. The LCP proteins present an important novel antibiotic target and may aid our understanding of assembly of heteropolymeric cell walls in fungi and plants.

Results

A role for MreB proteins in WTA synthesis or assembly

B. subtilis mutants affected in genes for lateral wall PG synthesis (*mreC*, *mreD*, *rodA*, and a double mutant of *pbpA* and *pbpH*) have a common phenotype in which the cells become spherical (Henriques *et al*, 1998; Wei *et al*, 2003; Leaver and Errington, 2005), and their growth requires high concentrations of Mg^{2+} (Supplementary Figure S1A). Mutants lacking all three *mreB* genes also adopt a spherical shape (Schirner and Errington, 2009; Kawai *et al*, 2009a) but they are not rescued by Mg^{2+} (Supplementary Figure S1A). Mutants affected in WTA synthesis are also spherical (Lazarevic and Karamata, 1995; Soldo *et al*, 2002; Bhavsar *et al*, 2004). We noticed that *tagG* and *tagH* mutants were, like the *mreB* triple mutant, unresponsive to Mg^{2+} (Supplementary Figure S1B). We hypothesized that the *mreB* triple mutant might be Mg^{2+}-unresponsive because the MreB cytoskeleton does not only control the Mg^{2+}-responsive PG synthesis, but additionally the Mg^{2+}-unresponsive WTA synthesis. To test this hypothesis, we made use of the unique feature of mutants affected in the later steps of WTA synthesis, which can be rescued by disruption of the *tagO* gene (D'Elia *et al*, 2006a, b). If this was correct, mutation of *tagO* might also suppress the lethality of triple *mreB* mutation. Figure 1A shows that disruption of *tagO* suppresses lethality in a conditional mutant in which the one remaining *mreB* homologue is under IPTG control, supporting the idea that the MreB proteins are required for one or more late steps in WTA synthesis.

The MreB cytoskeleton associates with known and novel components of the WTA biosynthetic machinery

We used *in vivo* cross-linking, followed by IMAC affinity copurification of oligohistidine-tagged MreB, Mbl, or MreBH, and liquid chromatography tandem mass spectrometry analysis (LC–MS/MS) to identify proteins associated with the MreB cytoskeleton. The list of proteins that pulled down with the cytoskeleton (summarized in Figure 2A, with full data for each of the isoforms in Supplementary Table SI) included various proteins already known to associate with MreB, such as PBP1, PBP2A, PBP4, PBPH, and MreC (Kawai *et al*, 2009a, b). Importantly, the list also included several proteins of the WTA pathway: TagD, TagE, TagF, and TagH, indicative of a role for the cytoskeleton in the synthesis or the assembly of WTA.

The WTA synthetic pathway of *B. subtilis* is the best characterized of any organism. However, although WTA polymer is known to be covalently linked to PG (Yokoyama *et al*, 1989), the transferase required for this reaction has not been identified. If the MreB protein was responsible for spatial organization of WTA, this factor should also be present in the MreB complexes. We analysed the list of candidates focusing on three key parameters: transmembrane (TM) topology, with a major (likely catalytic) domain predicted to be located outside the cytoplasm; gene location in proximity to known WTA synthetic loci (because WTA systems are variable and can be exchanged *en bloc* by genetic transformation) (Young *et al*, 1989); and phylogenetic distribution largely matching that of WTA. This analysis highlighted three members of the poorly characterized LCP family of genes and proteins (Figure 2). All three *B. subtilis* members of this gene family (*lytR*, *ywtF*, and *yvhJ*) are located within a 50-kbp segment of DNA that contains virtually all of the known WTA genes (Figure 2B). The three genes were renamed *tagT* (*ywtF*), *tagU* (*lytR*), and *tagV* (*yvhJ*).

Bacterial two-hybrid analysis revealed strong interactions between MreB and the TagT and TagU proteins (Supplementary Figure S2A). GFP fusions were made to each protein and expressed from the *amyE* locus under the control of a xylose-inducible promoter. GFP-TagU at least was functional based on a complementation tests (see below). Localization patterns of GFP-TagT and -TagU were reminiscent of those of MreB proteins, with patterns of distributed dots and tilted bands. These patterns were disrupted by double mutation of *mreB* and *mbl*, and by dissolution of the membrane potential, which Strahl and Hamoen (2010) recently showed was required for localization of MreB and associated proteins (Supplementary Figure S2C). GFP-TagV gave a less clear-cut pattern and the localization was not affected by *mreB* mutation or treatment with CCCP (Supplementary Figure S2C). These observations again support the idea that TagT and TagU, at least, are associated with the MreB cytoskeleton.

Triple disruption of the tagTUV genes causes loss of rod shape and is lethal under normal growth conditions

Single mutants of *tagT*, *tagU*, or *tagV* had no discernible effect on cell growth or morphology under normal growth conditions. To test for possible functional redundancy, all combinations of double mutants were then generated and confirmed to be viable. Δ*tagTU* and Δ*tagUV* mutants did not differ noticeably from the wild type (Figure 1B–D). However, the Δ*tagTV* mutant grew more slowly than the wild type and the cells were generally wider and often showed abnormal bulging (Figure 1E). A triple disruption of the *tagTUV* genes was apparently not viable. To investigate the phenotype of a triple mutant, *tagV* was placed under the control of the IPTG-inducible P_{spac} promoter in a Δ*tagTU* double mutant background. The resultant strain grew as normal rod-shaped cells in the presence of IPTG (Figure 1I). However, when IPTG was removed, growth was arrested and the morphology of the cells changed, becoming shorter and wider with noticeable abnormal bulging (Figure 1G), eventually becoming almost round (Figure 1H). Thus, at least one functional TagT, TagU, or TagV protein is required for viability and normal cell morphogenesis.

Disruption of the tagTUV genes can be suppressed by tagO mutation but not Mg^{2+}

If the *tagTUV* triple mutant was defective in WTA synthesis or assembly, it should be rescued by deletion of *tagO* but not by high Mg^{2+} concentration. As anticipated, growth of the triple

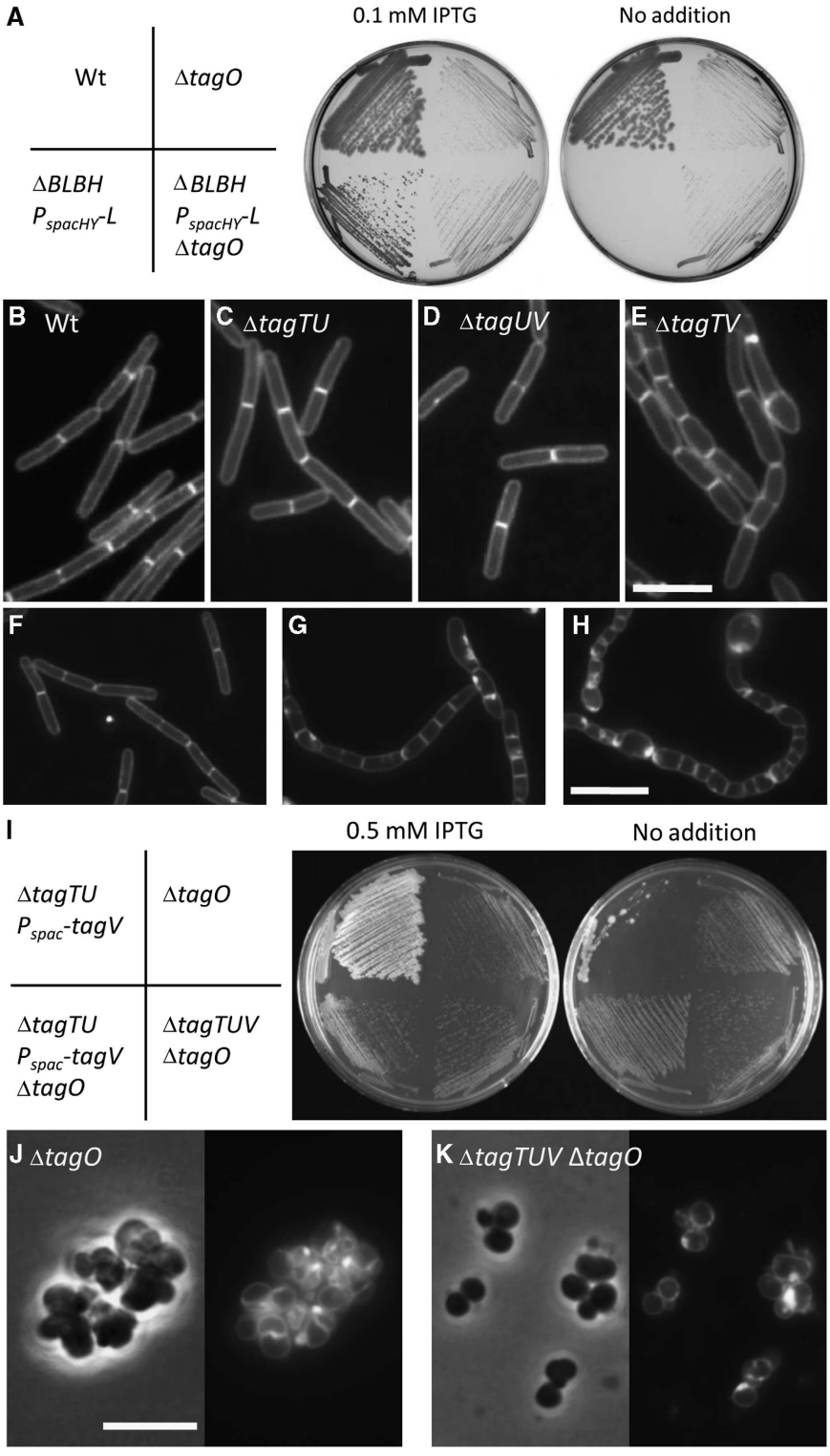

Figure 1 Lethal phenotype of a triple mutant of *mreB* paralogues and *tagTUV*, and rescue by disruption of *tagO*. (**A**) Growth of strains 168 (wild-type), YK992 (Δ*tagO*), YK1190 (*amyE*::P_{spacHY}-*mbl* Δ*mreB* Δ*mbl* Δ*mreBH* Δ*tagO*), and YK1119 (*amyE*::P_{spacHY}-*mbl* Δ*mreB* Δ*mbl* Δ*mreBH*) on NA plates with or without 0.1 mM IPTG. (**B**–**E**) Cell morphologies of typical fields of strains 168 (wild-type, **B**), RE204 (Δ*tagTU*, **C**), YK915 (Δ*tagUV*, **D**), and YK917 (Δ*tagTV*, **E**). The cell membranes were stained with Nile Red. Scale bar represents 5 μm. (**F**–**H**) Cell morphologies of typical fields of strain YK914 (Δ*tagTU* P_{spac}-*tagV*) cultured in the presence (**F**) or absence (**G**, **H**) of 0.5 mM IPTG. Images were taken at 180 (**G**) and 240 (**H**) min after removal of IPTG. The cell membranes were stained with Nile Red. Scale bar represents 5 μm. (**I**) Growth of strains YK1031 (Δ*tagTU* P_{spac}-*tagV* pMAP65), YK1030 (Δ*tagTU* P_{spac}-*tagV* Δ*tagO*), YK1033 (Δ*tagTUV* Δ*tagO*), and YK1163 (Δ*tagO*) on LB plates with or without 0.5 mM IPTG. (**J**, **K**) Cell morphologies of typical fields of strains YK1163 (Δ*tagO*, **J**) and YK1033 (Δ*tagTUV* Δ*tagO*, **K**). The cell membranes were stained with Nile Red (right). Scale bar represents 5 μm.

A

Category	Proteins detected
Cell shape and division	MreB, Mbl, MreBH, MreC, RodA, FtsE, FtsX, DivIVA, MinD, YluC
Cell envelope	AccC, FabF, YkuQ, GlmM, MurF, PBP1, PBP2A, PBP4, PBPH, DacA, TagD, TagE, TagF, TagH, DltD, YfnI
Unknown	LytR, SwrC, YckB, YdcG, YerH, YhbJ, YkaA, YkhA, YkrL, YlaG, YmcB, YneF, YpmB, YqbC, YqhL, YqhP, YqzC, YrrO, YsdC, YvbJ, YvhJ, YwtF, YxcE

B

Figure 2 The WTA biosynthetic machinery and LCP family of proteins associated with the MreB cytoskeleton. (**A**) Summary of proteins associated with MreB cytoskeleton (see also full data in Supplementary Table SI). WTA synthetic and LCP proteins are indicated in blue and red, respectively. (**B**) Genetic organization of three AP systems in *B. subtilis*, the WTA biosynthetic genes (blue), the teichuronic acid (TU) biosynthetic genes (green), and the minor TA biosynthetic genes (yellow). *lytR* homologues, *tagT*, *U*, and *V*, were indicated in red. Numbers show the position on the *B. subtilis* chromosome.

tagTUV mutant was not rescued by culture in the presence of various concentrations of Mg^{2+} up to 25 mM (Supplementary Figure S1C). We then took a null mutation of *tagO* and combined this with disruptions of the *tagT U* and *V* genes and P_{spac}-*tagV*. The resulting strain grew even in the absence of IPTG (Figure 1I), suggesting that disruption of *tagO* suppresses the lethality of *tagTUV* triple disruption. To confirm this, we were able to construct the quadruple mutant directly, taking advantage of the proximity of the *tagV* and *tagO* genes (see Supplementary data). The resulting strain was viable, and its morphological phenotype was indistinguishable from that of a *tagO* single mutant (Figure 1J and K).

TagTUV proteins are required for WTA synthesis or assembly

To test directly for a WTA defect, cell wall material (the insoluble PG–WTA complex) was isolated from various strains and acid treated to solubilize the WTA polymers, which were subsequently separated by PAGE and visualized by alcian blue-silver staining (Wolters *et al*, 1990) (Figure 3A). Extracts of the wild-type strain revealed the expected ladder-like pattern, representing partially hydrolysed WTA polymers with a range of distinct chain lengths (lanes 1 and 6). WTA material was completely absent from cells of the *tagO* mutant, in which the first step in the WTA pathway is blocked (lane 5). The staining pattern for the single *tagU* mutant was indistinguishable from that of the wild type (lane 2). When the triple *tagTUV* mutant containing the P_{spac}-*tagV* construct was grown in the presence or absence of IPTG, the amount of WTA polymer was greatly reduced in the absence of IPTG (lane 4) compared with its presence (lane 3), consistent with *tagV* being required for WTA accumulation in the wall. Residual WTA present in lane 4 is probably due to incomplete repression of the P_{spac} promoter in the samples.

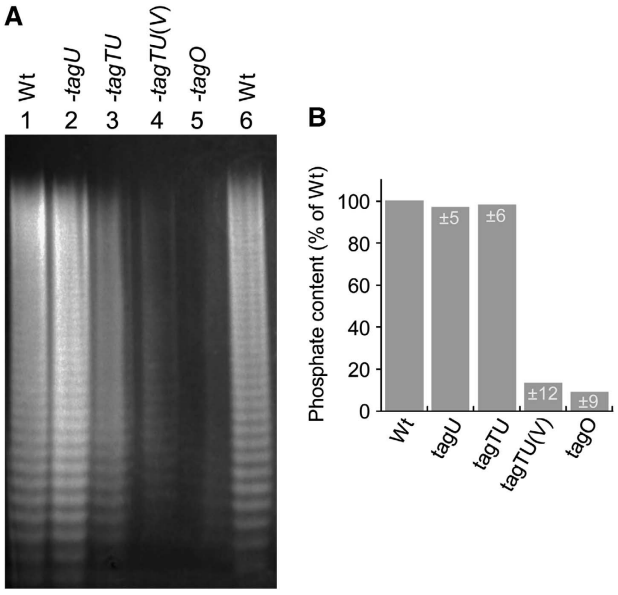

Figure 3 Effects of *tagTUV* mutants on WTA synthesis or assembly. (**A**, **B**) Cells of 168 (wild-type, lanes 1 and 6), RE201 (Δ*tagU*, lane 2), YK914 (Δ*tagTU* P_{spac}-*tagV*, lanes 3 and 4), and YK992 (Δ*tagO*, lane 5) were cultured with (lane 3) or without (lanes 1, 2 and 4–6) IPTG. Purified WTA samples were separated and visualized as described in the Materials and methods (**A**). Phosphate content of cell wall was assayed as described in the Materials and methods (**B**). White numbers indicate standard deviation from three independent experiments.

Cell wall phosphate, which is present only in WTA and is not found in PG, was also quantified in the various mutants (Figure 3B). Consistent with a previous report (Soldo *et al*, 2002; D'Elia *et al*, 2009), the wall phosphate content of the *tagO* null mutant was greatly reduced compared with wild-type cells. By contrast, the wall phosphate content of the *tagU* single mutant or the *tagTUV* triple mutant containing the

P_{spac}-*tagV* construct grown in the presence of IPTG had almost wild-type cell wall phosphate contents. However, in the absence of IPTG, wall phosphate was greatly reduced, almost to the levels found in the *tagO* mutant. We therefore concluded that TagTUV proteins have a critical function in the formation of a WTA-loaded cell wall.

The structure of ΔTM-Cps2A from Streptococcus pneumoniae

Attempts to develop direct biochemical assays for TagTUV activity, using mimics of the complex lipid-linked techoic acid substrate, were not successful in the first instance. To obtain molecular insights into the LCP family of proteins, and their likely enzymatic function, we screened a number of LCP proteins lacking the N-terminal, TM spanning region (ΔTM-) for crystallization. We solved the structure of the ΔTM version of the capsule synthesis protein CpsA from serotype 2 *S. pneumoniae* D39 (named ΔTM-Cps2A from here on) by selenomethionine SAD and refined the subsequent atomic model at 1.69 Å resolution (Supplementary Table SII).

ΔTM-Cps2A comprises two distinct domains: domain 1 (the accessory domain) comprises residues 111–213 and domain 2 (the LCP domain) spans residues 214–481 (Figure 4). The structure of the accessory domain, the sequence (and indeed the presence) of which is not conserved in the wider LCP family of proteins, is depicted in Figure 4A and B, and described in detail in Supplementary Figure S3. The LCP domain of ΔTM-Cps2A, which shares ~30% sequence identities with the equivalent domains from the three *B. subtilis* LCP proteins, is described below.

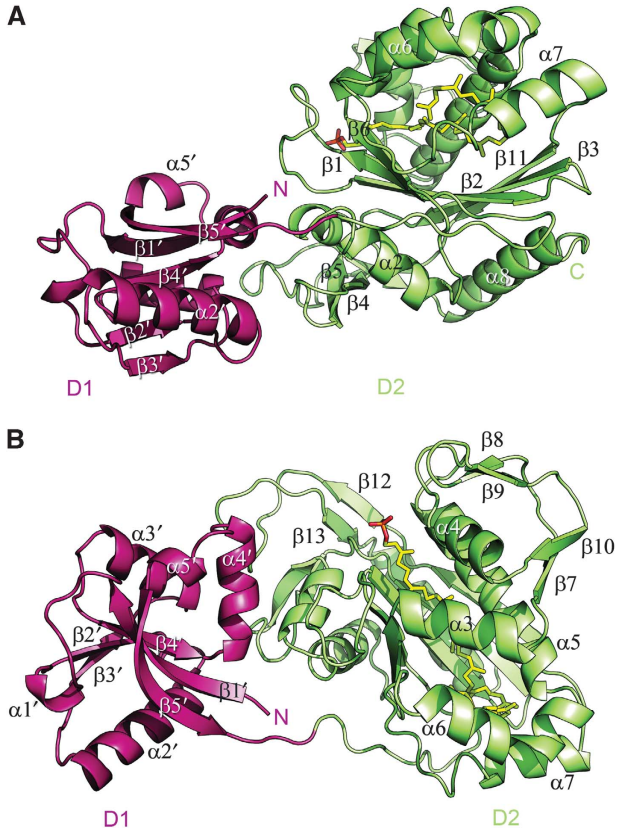

Figure 4 The structure of ΔTM-Cps2A. (**A**, **B**) Orthogonal views of the extracellular portion of Cps2A, shown as a cartoon, with the accessory domain coloured red and the LCP domain coloured green. The decaprenyl-phosphate present in the active site is shown as a stick model, with carbon atoms coloured yellow, phosphorous in orange, and oxygen in red. Secondary structure elements in both domains are labelled from N- to C-termini of each domain.

The LCP domain binds phosphorylated polyisoprenoid lipids

The LCP domain has an α–β–α architecture with a five-stranded β-sheet forming the core of the protein and α-helices surrounding the sheet on both faces (Figure 4). Two pairs of β-strands (β4/β5 and β12/β13) extend away from the protein core to form the interface between the two domains of ΔTM-Cps2A, burying some 570 $Å^2$ of surface area in the process. Crucially, a polyisoprenoid phosphate lipid was found in a hydrophobic pocket between the main β-sheet and α-helices α3–α7 (Figure 4). Presumably, ΔTM-Cps2A had bound the lipid when heterologously expressed in the *Escherichia coli* host, consistent with its affinity for a lipid-linked capsule precursor in *S. pneumoniae*. The lipid was built as mono-*trans*, octa-*cis* decaprenyl-phosphate (dpr-*P*).

We were subsequently able to solve the structure of ΔTM-Cps2A by molecular replacement in the presence of all *cis* octaprenyl-pyrophosphate (opr-*PP*) bound in the lipid-binding site. Again, no effort was made to load the protein with lipid prior to crystallization. The variation in lipid content between preparations of ΔTM-Cps2A probably represents a difference in the lipid composition of the two *E. coli* strains used: BL21 (DE3) leads to opr-*PP* being bound whereas B834 (DE3) results in dpr-*P* being bound. In both cases, the identity of the bound lipid was determined by electrospray mass spectroscopy of protein:lipid complexes. Mass differences between free proteins and lipid-bound proteins were 774 and 724 Da (Supplementary Figure S4A and B), corresponding to dpr-*P* and opr-*PP* (equivalent molecular masses 777 and 723 Da, respectively). The electron density maps prior to the building of the bound lipids, and during refinement, are consistent with the presence of dpr-*P* in one structure and opr-*PP* in the other. Both lipids are found naturally in bacteria (Bouhss *et al*, 2008).

The polyisoprenoid-binding pocket is lined with hydrophobic side chains (Figures 4 and 5A and C) from residues that, although not strictly identical, are completely conserved in hydrophobic character across the entire LCP family of proteins. The cavity for the lipid increases in diameter beyond the sixth isoprenoid, so much so that the lipid is folded back upon itself where the cavity for lipid binding is at its widest, and there are fewer interactions with the protein (Figure 5A and C). Consequently, the electron density in the region of the sixth prenoid moiety in both the dpr-*P* and opr-*PP* complexes is relatively poor, as is the electron density for the terminal prenoid group in the dpr-*P* structure. The key interactions between lipid and protein are, however, maintained in both structures (Figure 5A and C).

The phosphate headgroup of the dpr-*P* lipid is held in place by a number of conserved, charged residues. The invariant R267, R362, and R374 form key interactions with all the phosphate oxygens to form a positively charged pocket in the protein surface (Figure 5B). The conserved D371 and Q378 are in contact with these arginine residues to stabilize further their conformations.

The lipid-proximal phosphate in the opr-*PP*-bound structure is shifted slightly and now makes contacts to D234,

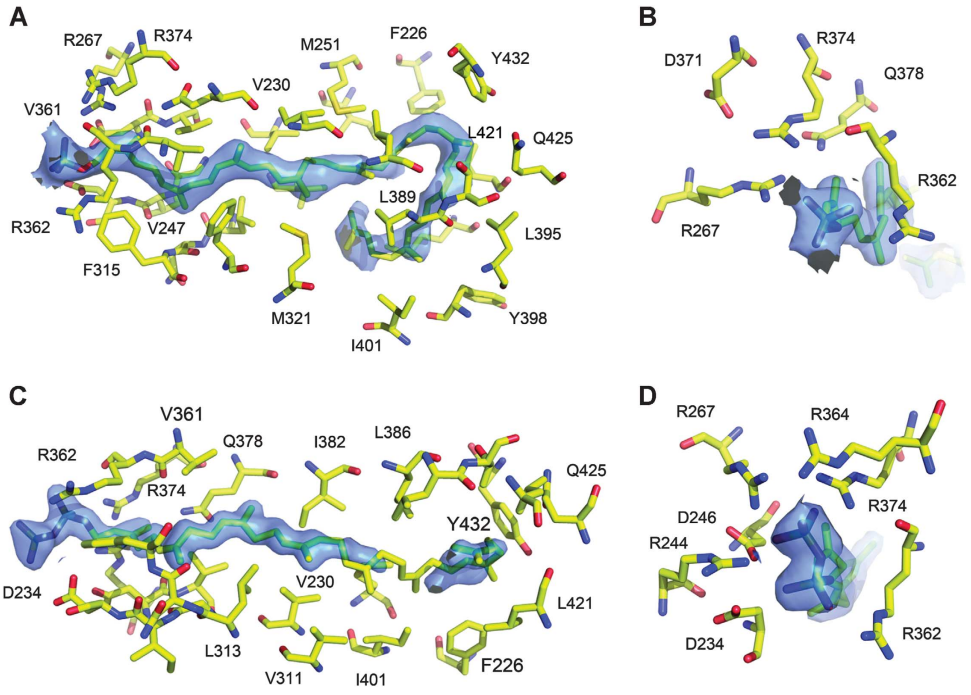

Figure 5 Lipid binding by the LCP domain of ΔTM-Cps2A. (**A**, **B**) decaprenyl-phosphate binding to ΔTM-Cps2A and (**C**, **D**) octaprenyl-pyrophosphate bound ΔTM-Cps2A. Protein residues within 4 Å of the lipid are shown as stick models, with final, σ^A-type $2mF_{obs}–DF_{calc}$ electron density maps shown as blue transparent surfaces and contoured in both cases at 1.0 σ.

R244, and R362, whereas the lipid-distal phosphate contacts the invariant arginines, R244, R267, R364, and R374, fixing the position and orientation of the pyrophosphate (Figure 5D). In the dpr-*P* structure, R267 is built in two conformations, only one of which interacts with the phosphate. Similarly, in the dpr-*P* structure, R244 and R364 point into solvent, but, as with R267, readjust their conformations in the presence of a pyrophosphate lipid headgroup.

Since the structure solution of ΔTM-Cps2A, seven unpublished outputs from the Northeast Structural Genomics Consortium have been deposited in the PDB that likely represent structures of other LCP proteins. None of these entries have been characterized biochemically or genetically. These structures (PDBids: 3PE5 (from *Clostridium leptum*, UNIPROT code A7VV38); 3QFI (*Enterococcus faecalis*, Q838I2); 3OWQ (*Listeria innocua*, Q92CZ6); 3NXH (*B. subtilis*, P96499); 3NRO (*Listeria monocytogenes*, Q8Y889); 3OKZ (*Streptococcus algalactiae*, Q8E703), and 3MEJ (*B. subtilis*, Q7WY78)) are the only meaningful homologues to ΔTM-Cps2A that can be found in the PDB by either secondary structure matching or amino-acid sequence searches and they are mostly, and apparently incorrectly, annotated as transcriptional regulators, whereas there is no significant structural homology of these structures, or of ΔTM-Cps2A, to known transcription factors in the PDB. The range of sequence identities of the seven hits, in comparison to the catalytic domain of Cps2A, is between 29 and 32% with BLAST *E*-values between 5^{-23} and 8^{-16}. All but one (3PE5) can be superimposed on ΔTM-Cps2A with r.m.s.d.s of 1.8–2.2 Å on 200–230 matched Cα atoms of the catalytic domain (for 3PE5, the r.m.s.d. is 2.8 Å on 224 matched Cαs). None of these seven PDBs contain bound lipid, despite the close sequence and structural homology in global terms, and in the regions of the proteins that bind the lipid. The hydrophobic residues in ΔTM-Cps2A that are within van der Waals' contact of the bound isoprenoid lipids have hydrophobic amino acids in the equivalent positions in the other available structures. The charged amino acids in ΔTM-Cps2A in the vicinity of the pyrophosphate headgroup are almost completely invariant in the other structures (Supplementary Figure S5). Consequently, it is not evident why ΔTM-Cps2A should purify from *E. coli* with lipids bound, whereas the other LCP proteins do not.

The LCP proteins likely catalyse a missing step in cell wall synthesis

Anionic (or acidic) polymers, for instance teichoic acids or capsular polysaccharides, are synthesized inside the cell, and are attached to a carrier lipid, undecaprenyl phosphate for translocation ('flipping') to the outside of the cell. In the final stage of the biosynthesis of the cell wall of bacteria, teichoic acids are covalently attached to PG, whereby the structure of the acceptor (PG precursor, nascent PG chain, or cross-linked PG) is not known. This phosphotransfer reaction links the phospho-teichoic acid chain to PG MurNAc residues releasing undecaprenyl phosphate PG whereby. Our structural and genetic data suggest that the LCP proteins catalyse this step.

The observation of polyisoprenyl (pyro)phosphate lipids bound to ΔTM-Cps2A identified the active site for the entire LCP family (Supplementary Table SIII). The roles of key, conserved amino acids in the lipid-binding pocket were confirmed by mutagenesis of the *B. subtilis tagU* gene (see below and Figure 6A).

LCP proteins are magnesium-dependent phosphotransferases

The importance of the two aspartic acids was clarified by our discovery that D234 and D246 coordinate a magnesium ion

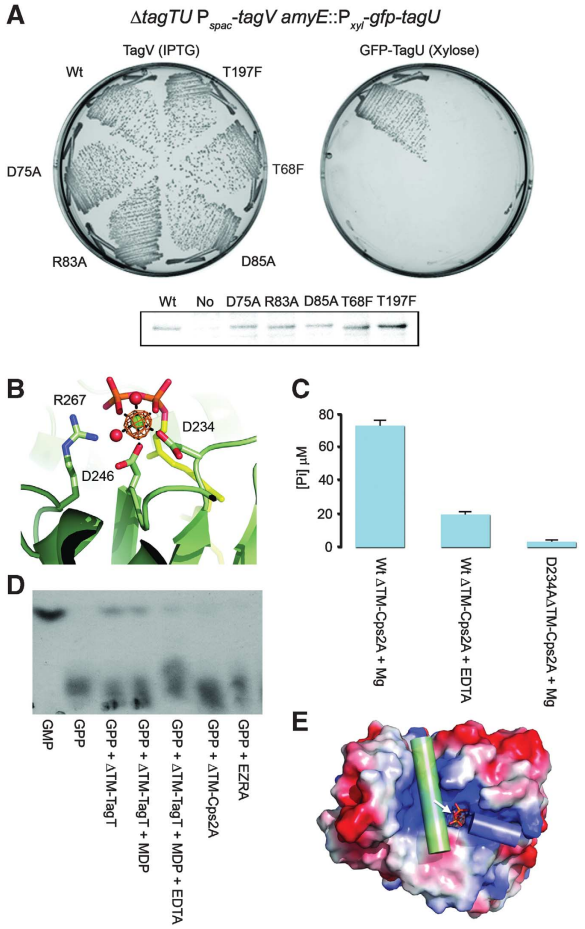

Figure 6 The biochemical properties of LCP proteins. (**A**) Growth of strains YK1254 (wild-type GFP-TagU), YK1365 (D75A), YK1366 (R83A), YK1367 (D85A), YK1368 (T86F), and YK1369 (T197F) on NA plates with 0.5 mM IPTG or 0.5% xylose. Western blot analysis of GFP-TagU levels in strain expressing wild-type and various mutant GFP-TagU fusions with or without (No) 0.5% xylose indicate correct accumulation of the proteins and consequently mutations D75A, R83A, D85A, T86F, and T197F in TagU are unable to sustain growth in the absence of wild-type copy of *tagT*, *tagU*, and *tagV*. (**B**) Metal binding by ΔTM-Cps2A. Crystals of Cps2A soaked in manganese show a clear peak in an anomalous difference map calculated for data collected at the manganese *K*-edge (orange mesh). Metal coordinating residues are shown as ball and stick representations, with the position of R267A shown with blue carbons. (**C**) Incubation of ΔTM-CPS2A–octaprenyl-pyrophosphate complex with magnesium releases inorganic phosphate. Addition of EDTA, or mutation to alanine of aspartate 234, which coordinates the catalytic magnesium ion, both suppress release of inorganic phosphate. Bar length is proportional to the wild-type experiment with Mg^{2+} present (76.31 ± 2.9 μM released with Mg^{2+} present versus 20.60 ± 1.26 μM released with EDTA present; 3.38 ± 0.68 released by D234A). (**D**) Pyrophosphatase activity of ΔTM-TagT. A purified ΔTM-TagT protein catalyses hydrolysis of the pyrophosphate bond in exogenously added geranyl pyrophosphate (ger-*PP*) to generate geranyl monophosphate (ger-*P*), monitored by thin layer chromatography. Parallel incubations with the unrelated protein, EzrA (purified using the same procedures as the LCP proteins herein) and ΔTM-Cps2A reveal no pyrophosphatase activity towards exogenous ger-*PP*; in the latter case, this can be attributed to the blockage of the active site by endogenous opr-*PP* lipid. Hydrolysis is magnesium dependent, but is not affected by the addition of the PG fragment, *N*-acetylmuramyl dipeptide (MDP). (**E**) Electrostatic protein surface of the LCP domain of ΔTM-Cps2A, with bound octaprenyl-pyrophosphate ligand. The scissile bond in the phosphotransferase reaction catalysed by this enzyme class is shown with an arrow. The potential pathway for AP binding is highlighted in blue, semi-transparent rod (labelled AP), and the likely position of PG, to which the phosphorylated AP will be transferred, is shown with the green rod (labelled PG).

that is situated between the two phosphate groups of opr-*PP* in a further structure of ΔTM-Cps2A (Figure 6B). The presence of opr-*PP* in the sample was confirmed by mass spectrometry. The assignment of magnesium in the structure was confirmed by a separate structure determination of ΔTM-Cps2A–R267A–opr-*PP* with manganese bound, where the position of the bound metal ion was verified in an anomalous difference Fourier (Figure 6B, and the identity of the bound lipid by mass spectrometry; Supplementary Figure S4C). The bound Mg^{2+} obeys near perfect octahedral geometry, with one ligand each from D234, D246 and oxygens from both phosphates (Figure 6B). The other two coordination positions are filled by water molecules. The side chain of R244 is displaced by the binding of divalent cations, and no longer interacts with the pyrophosphate headgroup. Otherwise, the interactions with the opr-*PP* lipid are the same as in the absence of the metal, including the abuttal of the distal phosphate by the side chain of R267 (Figure 5D), which presumably aids catalysis by stabilizing the transition state.

The role of magnesium in catalysis was investigated with a colourimetric assay to measure the liberation of free phosphate from ΔTM-Cps2A that had been purified with opr-*PP* bound, to demonstrate the capacity of ΔTM-Cps2A to cleave the phosphoester bond in pyrophosphate-containing lipids. In this assay, the absence of Mg^{2+} ions from the reaction, or the presence of EDTA, produced significantly less P_i in an end point assay than when Mg^{2+} ions were present (Figure 6C). Similarly, removal of one of the key Mg^{2+} coordination partners, D234, by its mutation to alanine produced significantly less free P_i when incubated in the presence of Mg^{2+} (Figure 6C). The key role for the Mg^{2+} coordination by D234 is consistent with our observation that a *B. subtilis* TagU carrying the equivalent mutation, D75A, is not functional *in vivo* (Figure 6A; Supplementary Table SIII).

In contrast to ΔTM-Cps2A, purified preparations of *B. subtilis* ΔTM-TagT were not loaded with an *E. coli* lipid, as confirmed by X-ray crystallography, and catalysed the hydrolysis of the pyrophosphate phosphoester bond in an exogenously added lipid, geranyl pyrophosphate (ger-*PP*), in a magnesium-dependent manner (Figure 6D). The addition of high molecular weight PG, or of a small PG fragment, *N*-acetylmuramyl dipeptide, did not stimulate the transfer of the terminal phosphoryl group to the possible acceptor. Most likely, the reaction catalysed by the LCP proteins favours phosphotransfer from AP-loaded substrates (which are not commercially available), over that from the unloaded diphosphoryl lipid substrate present in our reaction. Nonetheless, our *in vivo* and *in vitro* data strongly suggest that the LCP family of proteins is the missing enzyme that catalyse the linkage of teichoic acids and other acidic/APs to PG.

Discussion

LCP proteins are phosphotransferases

Studying the final step of bacterial cell wall synthesis, the attachment of TA to PG, has been proven very challenging to multiple laboratories for several reasons: (i) the substrates have highly complex, heterogeneous structures that are not commercially available, (ii) the precise identity of the PG acceptor (precursor, nascent chain, or cross-linked polymer) is not known, and (iii) the reaction is catalysed at the

cytoplasmic membrane by integral membrane proteins and is likely linked to membrane transport of the precursors. Although we could not reconstitute this complex system *in vitro*, in this paper, we present data that, in combination, strongly suggest that members of the LCP family of proteins are the long searched for enzymes that attach APs to cell wall PG. This conclusion is based on the following observations: (i) the TagTUV paralogues have a role in a late step WTA synthesis in *B. subtilis* as shown by genetics and by measurements of the WTA content of a triple mutant strain; (ii) the cocrystal structures of *S. pneumoniae* Cps2A containing bound substrate and product analogues that are consistent with the missing enzymatic step; (iii) our demonstration that TagT and Cps2A can both produce a monophosphorylated lipid from a diphosphorylated substrate in a Mg^{2+}-dependent fashion; (iv) the observation of a Mg^{2+} ion in a location indicating a role in phosphorolysis; and (v) mutation of key amino acids in lipid and Mg^{2+} binding blocks the *in vitro* phosphorolysis and abolishes function *in vivo*. Consistent with this conclusion, LCP genes found in AP-containing Gram-positive bacteria are always located in close proximity, often in the same operon, to genes required for AP synthesis. Furthermore, mutants lacking members of the LCP family have been isolated in a number of different bacteria, and in many cases, these mutants have altered cell wall structures, autolysin activities, lower antibiotic resistance levels and/or reduced virulence (Hübscher *et al*, 2008, 2009). Because of these pleiotropic effects, some members of the family were suggested to have a regulatory role in cell wall growth, and the situation is complicated further by the presence in *S. aureus* of a transcriptional activator named LytR that shows no sequence similarity to LCP proteins (Brunskill and Bayles, 1996). The short cytoplasmic regions of a Cps2A homologue from *Streptococcus iniae* were shown to bind DNA *in vitro* (Hanson *et al*, 2011). In addition, early work on the *B. subtilis lytR* gene suggested a role in transcriptional regulation because disruption of *lytR* resulted in increased transcription of both *lytR* and the adjacent *lytABC* operon (Lazarevic *et al*, 1992). However, our work does not support a regulatory role for the LCP proteins. Presumably, many of the published phenotypes of LCP mutant strains of the various species studied are indirect consequences of major cell wall alterations and the resulting stress response due to failure of the attachment of APs to PG.

We were unable to detect free APs in the supernatant of the triple *tagTUV* depletion strain (RAD, unpublished data). Indeed, several previous reports have documented a reduction of cell wall-attached APs in LCP mutants of various bacterial species (Massidda *et al*, 1996; Cieslewicz *et al*, 2001; Morona *et al*, 2006; Hübscher *et al*, 2009). It seems possible that feedback regulation blocks the synthesis and or export of APs when the attachment to PG is impaired.

Implications for the phosphotransferase mechanism catalysed by LCP proteins

The LCP proteins presumably attach teichoic acid, teichuronic acid, or acidic capsular polysaccharide to cell wall PG via phosphodiester linkage to *N*-acteylmuramic acid. Our data on the three *B. subtilis* homologues indicate that the enzymes are not absolutely specific for the type of AP, teichoic acid, or teichuronic acid they attach, because a major phenotype does not emerge until all three genes are inactivated. This is supported by our crystal structures of Cps2A in complex with reaction product and substrate mimics, which indicate that the enzymes interact strongly with the pyrophosphoryl-lipid component of the AP precursor. There is space in the crystal structure beyond the terminal phosphate of the bound opr-*PP* to accommodate the oligosaccharide moiety that links the lipid to the acidic/AP component. Important interactions with the sugar that is linked directly to the pyrophosphate might occur from the conserved arginine pair, Arg362 and Arg244 of Cps2A. The first two carbohydrate residues of the AP, called the linkage unit, would project into a cleft on the surface of ΔTM-Cps2A (Figure 6E) and the rest of the polymeric, main chain component of the AP precursor is unlikely to interact with the protein. Thus, teichoic/teichuronic acid-attaching enzymes would only recognize the linkage unit of the precursor and not the main chain explaining the lack of specificity of the *Bacillus* enzymes. The PG polymer could be accommodated in the groove above β-strands 18 and 19 (Figure 6E). While we have been able to demonstrate the phosphorolysis of the scissile bond in a substrate mimic, we have not been able to detect phosphotransfer to a PG acceptor. Perhaps, the carbohydrate linkage unit participates in catalysis, by interacting with conserved arginines. If interactions between the linkage unit of AP and protein atoms of the LCP enzyme are crucial to the biochemical reaction, it would help to explain why phosphotransfer efficiency is poor with just a phosphate anion as a leaving group; after all, the reaction trajectories for phosphate monoesters differ fundamentally from those of phosphate di- and tri-esters (Cleland and Hengge, 2006).

The crystal structures provide several clues towards the likely catalytic mechanism. First, Mg^{2+} appears to be an essential catalytic requirement. The divalent cation and the presence of several conserved arginines (e.g. Arg244, Arg267, and Arg362; Figure 5) may contribute to catalysis by stabilizing the transition state by the neutralization of the developing negative charge. Second, there is no obvious amino acid to act as a base in the activation of the incoming nucleophile. There are two acidic groups close to the scissile bond, but both these, Asp234 and Asp246, coordinate the bound magnesium. The coordination of the cation by these two acidic amino acids, and the interaction of phosphate groups with neighbouring positively charged amino acids, is reminiscent of the reaction scheme catalysed by acyl carrier protein (ACP) synthase (Bunkoczi *et al*, 2007). That residues Glu181 and Lys185 participate in general acid and base catalysis in ACP synthase were confirmed by mutagenesis. Possible functional equivalents in Cps2A are Asp234, demonstrated herein to be a crucial amino acid for LCP function, and Arg362, one of several conserved positively charged residues coordinating the pyrophosphate. An alternative candidate to act as the catalytic base is the conserved Asp268, but this is about 5 Å away from the likely position of the incoming nucleophile. Significant conformational changes would be needed to locate this amino acid in a position to extract a proton from phosphotransfer acceptor. Other phosphotransfer reactions do, however, take place without the need for a classic general acid/base pair (Cleland and Hengge, 2006). Finally, the metal ion itself may activate the nucleophilic hydroxyl moiety (Lassila *et al*, 2011) as the phosphoacceptor approaches the active site in order to provide the necessary rate enhancement expected of an enzyme.

We have been unable to visualize the interactions of PG and AP building blocks with the protein, primarily because of the unavailability of some complex substrate components, but also because the active site of Cps2A is already blocked with lipids. It remains to be shown how the lipid is loaded and released from the protein *in vivo*. Perhaps, the phospholipids of the cell membrane can passively empty the enzyme active site without recourse to another protein. Alternatively, the product of the transfer reaction, a monophosphorylated polyisoprenoid lipid might be actively removed from the active site, by an as yet unidentified protein, to be 'flipped' back across the membrane to its inner face so that the phospholipid can be recharged by the cytoplasmic Tag pathway for the enzyme to perform another round of phosphotransfer.

Fungi and plants also covalently attach polysaccharides and other polymers to the primary cell wall but the enzymes catalysing the attachment are not yet known, nor are the mechanisms of spatiotemporal regulation of these processes understood (McNeil *et al*, 1984; Latge, 2007). Thus, our work could stimulate further studies of the assembly of complex cell walls in other organisms.

Global role of the MreB cytoskeleton in coordinating synthesis and assembly of a range of different cell wall polymers

Synthesis of both PG and WTA is concentrated at a central growth zone in *S. pnuemoniae* (Tomasz *et al*, 1975), a bacterium that does not contain an MreB cytoskeleton. The discovery of the TagTUV proteins, other WTA proteins, and PG synthetic enzymes in association with the three MreB proteins reinforces the idea that in rod-shaped bacteria, the cytoskeleton orchestrates the activity of not just the PG-synthesizing machinery but also a range of other cell wall components. In support of this idea, several enzymes of both the PG and WTA synthetic machineries have a pattern of localization that appears similar to that of the MreB proteins (Scheffers *et al*, 2004; Claessen *et al*, 2008; Formstone *et al*, 2008) (Supplementary Figure S2). Close association of the PG- and WTA-synthesizing machineries with the MreB proteins could provide a means of coordinating the insertion of WTA with the deposition of PG. Therefore, these results lend strong support to the emerging picture that the MreB cytoskeleton plays a pivotal role in organizing and coordinating the different elements of cell envelope morphogenesis in bacteria.

A novel antibiotic target

Several authors have speculated about the WTA biosynthetic pathway as a potential antibiotic target (for a review, see Swoboda *et al*, 2010). Indeed, Swoboda *et al* (2009) have used a cell-based screen to identify a specific inhibitor of the WTA pathway in *S. aureus*, which was shown to work on the ABC transporter orthologous to TarG in *B. subtilis*. Since the active site of the putative transferase lies outside the cytoplasmic membrane, potential antibiotics targeted on this enzyme would have the advantage of not needing to cross the cytoplasmic membrane. This external location is one of the reasons why β-lactams, targeting the penicillin-binding proteins, have been so successful. Our discovery of the transferase responsible for transfer of nascent WTA to the PG, together with structural information on the substrate and clues to the likely catalytic mechanism, provides a highly attractive new target for drug discovery programmes.

Materials and methods

Complete details of all the materials and methods used are provided in the Supplementary data.

Bacterial strains, plasmids, and primers

Strains and plasmids used in this study are listed in Supplementary Table SIV and primers are listed in Supplementary Table SV. The construction of plasmids is described in the Supplementary data.

Media

Cultures of *Bacillus* strains were grown in Luria–Bertani (LB) or Difco antibiotic medium 3 (PAB) liquid at 30 or 37 °C, or on LB or nutrient agar (Oxoid) plates at 37 °C, with appropriate supplements when necessary.

Microscopic imaging

For fluorescence microscopy, cells from overnight cultures were diluted into fresh PAB medium and grown to mid-exponential phase at 30 °C. For live cell imaging, cells were mounted on microscope slides covered with a thin film of 1.2% agarose in water, essentially as described previously (Glaser *et al*, 1997). Images were acquired with a Sony Cool-Snap HQ cooled CCD camera attached to a Zeiss Axiovert 200 M microscope. The images were acquired and analysed with METAMORPH version 6 (Molecular Devices).

Purification of protein complexes

Proteins that copurified from liquid cultures of *B. subtilis* expressing MreB-, Mbl-, or MreBH-His were purified as described previously (Ishikawa *et al*, 2006; Kawai *et al*, 2009b). After separation by electrophoresis, polyacrylamide gels were divided into slices, and the presence of proteins confirmed by peptide-mass fingerprinting as described previously (Kuwana *et al*, 2002). As a negative control, cells expressing His-tagged Noc, a chromosome-associated negative regulator of cell division (Wu *et al*, 2009), were also analysed. Several proteins were simultaneously identified in both MreB and Noc complexes (e.g. TufA and ribosomal proteins), suggesting that they represent a non-specific background.

Extraction of cell wall material

B. subtilis cell cultures were grown in LB to late exponential phase ($OD_{600} = 0.7$). The cells were harvested, suspended in water, and then immediately added to 10 volumes of 4% SDS at 100 °C. After 20 min incubation, the cell wall material was washed with water 10 times, to remove the SDS. The resultant crude preparation was then suspended in 0.5% NaCl and broken using a bead beater (Bio101 unit at max power for 30 s). After removing the glass beads, the suspension was sedimented by centrifugation, and then washed with water 10 times. The cell wall material was freeze dried in preweighed tubes and to each tube an appropriate amount of water was added to equalize the concentration in each sample. Organic phosphorous was assayed as described previously (Harwood *et al*, 1990).

Electrophoresis of teichoic acids

Purified cell wall samples were treated with 1 M HCl for 20 min at 65 °C and then neutralized with NaOH. Glycerol was added to each hydrolysed sample to give a final concentration of 5%, along with bromophenol blue (0.001% final concentration). Samples were electrophoresed at 10 V/cm on a 12% polyacrylamide gel made in 1.2 × TBE buffer. The gel was stained with Alcian Blue, followed by silver staining, as described previously (Wolters *et al*, 1990).

Protein expression and purification for crystallization

Recombinant ΔTM-Cps2A (residues 98–481, with a C-terminal hexahistidine tag) was produced in the methionine auxotroph B834 (DE3) strain of *E. coli*. Cells were grown in LB media to an OD_{600} of 0.4 and induced with 1 mM IPTG for 18 h at 16 °C for native protein, or in minimal medium supplemented with selenomethionine for the seleno-labelled protein. Recombinant protein was purified as described in the Supplementary data.

Crystallization, structure determination, and refinement of ΔTM-Cps2A

Crystals of ΔTM-Cps2A were obtained by sparse-matrix screening from purified protein at 28 mg/ml. Diffraction data, collected at the Diamond Light Source were processed with MOSFLM (Leslie, 2006) and scaled with SCALA (Evans, 2006). The structure was solved using SHELX (Sheldrick, 2010) within HKL2MAP (Pape and Schneider, 2004); initial model building was performed using ARP/wARP (Langer *et al*, 2008). Refinement proceeded with cycles of automated refinement in PHENIX (Adams *et al*, 2010) and manual rebuilding in COOT (Emsley *et al*, 2010). Details of the diffraction data and refined models are reported in Supplementary Table SII.

Mass spectroscopy of ΔTM-Cps2A

Mass spectroscopy of ΔTM-Cps2A was performed on a Waters LCT Premier XE, using electrospray ionization in both native and denatured states.

Accession codes

Atomic co-ordinates and native structure factors have been deposited at the PDB for the wild type complexes with dpr-*P*, opr-*PP* and opr-*PP*/magnesium and for the R267A mutant of ΔTM-Cps2A in complex with opr-*PP* and manganese with respective accession codes 2xxp, 3tfl, 3tep and 3tel.

Supplementary data

Supplementary data are available at *The EMBO Journal* Online (http://www.embojournal.org).

Acknowledgements

This work was supported by a grant from the UK Biotechnology and Biological Sciences Research Council to JE, RAD, WV, and RJL. We thank the various group members for helpful discussions, and particularly Leendert Hamoen, Susan Firbank, and Romain Mercier for critical reading of the manuscript and Alice Eberhardt for help with cloning of *cps2A*. We also thank Hiroki Yamamoto, Junichi Sekiguchi, Mark Leaver, and Takuya Morimoto for the gift of strains, and Didier Blanot for gift of undecaprenyl phosphate standard, and Dan Herschlag for communicating a preprint of his review before publication. We also acknowledge the Diamond Light Source for access to its beamlines, the beamline staff and Arnaud Baslé for support during diffraction data collection. We also thank Adam Dowle, Andrew Leech, and Berni Strongitharm of the York University Technology Facility for mass spectroscopic analyses. The authors extend their condolences to the family of Berni Strongitharm, who sadly passed away in May 2011.

Author contributions: RE, SI, MK, NH, NKB, and CNH performed the experiments. YK, JM-W, and RMC designed and performed the experiments, analysed the data, and contributed to the drafting of the paper. NO contributed to the design of the experiments. RJL, WV, RAD, and JE contributed to the planning of the experiments, interpretation of data, and drafting of the paper.

Conflict of interest

The authors declare that they have no conflict of interest.

References

Adams PD, Afonine PV, Bunkoczi G, Chen VB, Davis IW, Echols N, Headd JJ, Hung LW, Kapral GJ, Grosse-Kunstleve RW, McCoy AJ, Moriarty NW, Oeffner R, Read RJ, Richardson DC, Richardson JS, Terwilliger TC, Zwart PH (2010) PHENIX: a comprehensive Python-based system for macromolecular structure solution. *Acta Crystallogr D Biol Crystallogr* **66:** 213–221

Atilano ML, Pereira PM, Yates J, Reed P, Veiga H, Pinho MG, Filipe SR (2010) Teichoic acids are temporal and spatial regulators of peptidoglycan cross-linking in *Staphylococcus aureus*. *Proc Natl Acad Sci USA* **107:** 18991–18996

Bhavsar AP, Erdman LK, Schertzer JW, Brown ED (2004) Teichoic acid is an essential polymer in *Bacillus subtilis* that is functionally distinct from teichuronic acid. *J Bacteriol* **186:** 7865–7873

Bouhss A, Trunkfield AE, Bugg TD, Mengin-Lecreulx D (2008) The biosynthesis of peptidoglycan lipid-linked intermediates. *FEMS Microbiol Rev* **32:** 208–233

Brown S, Zhang YH, Walker S (2008) A revised pathway proposed for *Staphylococcus aureus* wall teichoic acid biosynthesis based on *in vitro* reconstitution of the intracellular steps. *Chem Biol* **15:** 12–21

Brunskill EW, Bayles KW (1996) Identification and molecular characterization of a putative regulatory locus that affects autolysis in *Staphylococcus aureus*. *J Bacteriol* **178:** 611–618

Bunkoczi G, Pasta S, Joshi A, Wu X, Kavanagh KL, Smith S, Oppermann U (2007) Mechanism and substrate recognition of human holo ACP synthase. *Chem Biol* **14:** 1243–1253

Carballido-Lopez R, Formstone A, Li Y, Ehrlich SD, Noirot P, Errington J (2006) Actin homolog MreBH governs cell morphogenesis by localization of the cell wall hydrolase LytE. *Dev Cell* **11:** 399–409

Cieslewicz MJ, Kasper DL, Wang Y, Wessels MR (2001) Functional analysis in type Ia group B *Streptococcus* of a cluster of genes involved in extracellular polysaccharide production by diverse species of streptococci. *J Biol Chem* **276:** 139–146

Claessen D, Emmins R, Hamoen LW, Daniel RA, Errington J, Edwards DH (2008) Control of the cell elongation-division cycle by shuttling of PBP1 protein in *Bacillus subtilis*. *Mol Microbiol* **68:** 1029–1046

Cleland WW, Hengge AC (2006) Enzymatic mechanisms of phosphate and sulfate transfer. *Chem Rev* **106:** 3252–3278

D'Elia MA, Henderson JA, Beveridge TJ, Heinrichs DE, Brown ED (2009) The N-acetylmannosamine transferase catalyzes the first committed step of teichoic acid assembly in *Bacillus subtilis* and *Staphylococcus aureus*. *J Bacteriol* **191:** 4030–4034

D'Elia MA, Millar KE, Beveridge TJ, Brown ED (2006a) Wall teichoic acid polymers are dispensable for cell viability in *Bacillus subtilis*. *J Bacteriol* **188:** 8313–8316

D'Elia MA, Pereira MP, Chung YS, Zhao W, Chau A, Kenney TJ, Sulavik MC, Black TA, Brown ED (2006b) Lesions in teichoic acid biosynthesis in *Staphylococcus aureus* lead to a lethal gain of function in the otherwise dispensable pathway. *J Bacteriol* **188:** 4183–4189

Daniel RA, Errington J (2003) Control of cell morphogenesis in bacteria: two distinct ways to make a rod-shaped cell. *Cell* **113:** 767–776

Emsley P, Lohkamp B, Scott WG, Cowtan K (2010) Features and development of Coot. *Acta Crystallogr D Biol Crystallogr* **66:** 486–501

Evans P (2006) Scaling and assessment of data quality. *Acta Crystallogr D Biol Crystallogr* **62:** 72–82

Figge RM, Divakaruni AV, Gober JW (2004) MreB, the cell shape-determining bacterial actin homologue, co-ordinates cell wall morphogenesis in *Caulobacter crescentus*. *Mol Microbiol* **51:** 1321–1332

Formstone A, Carballido-Lopez R, Noirot P, Errington J, Scheffers DJ (2008) Localization and interactions of teichoic acid synthetic enzymes in *Bacillus subtilis*. *J Bacteriol* **190:** 1812–1821

Formstone A, Errington J (2005) A magnesium-dependent *mreB* null mutant: implications for the role of *mreB* in *Bacillus subtilis*. *Mol Microbiol* **55:** 1646–1657

Foster SJ, Popham DL (2002) Structure and synthesis of cell wall, spore cortex, teichoic acids, S-layers, and capsules. In *Bacillus subtilis and Its Closest Relatives: From Genes to Cells*, Sonenshein L, Losick R, Hoch JA (eds) pp 21–41. Washington, DC: American Society for Microbiology

Glaser P, Sharpe ME, Raether B, Perego M, Ohlsen K, Errington J (1997) Dynamic, mitotic-like behavior of a bacterial protein required for accurate chromosome partitioning. *Genes Dev* **11:** 1160–1168

Graumann PL (2009) Dynamics of bacterial cytoskeletal elements. *Cell Motil Cytoskeleton* **66:** 909–914

Hanson BR, Lowe BA, Neely MN (2011) Membrane topology and DNA-binding ability of the *Streptococcal* CpsA protein. *J Bacteriol* **193:** 411–420

Harwood CR, Coxon RD, Hancock IC (1990) The *Bacillus* cell envelope and secrition. In *Molecular Biology Methods for Bacillus*, Harwood CR, Cutting SM (eds) pp 328–369. New York City: John Wiley & Sons Ltd

Henriques AO, Glaser P, Piggot PJ, Moran Jr CP (1998) Control of cell shape and elongation by the *rodA* gene in *Bacillus subtilis*. *Mol Microbiol* **28:** 235–247

Hu B, Yang G, Zhao W, Zhang Y, Zhao J (2007) MreB is important for cell shape but not for chromosome segregation of the filamentous cyanobacterium *Anabaena sp*. PCC 7120. *Mol Microbiol* **63:** 1640–1652

Hübscher J, Luthy L, Berger-Bachi B, Stutzmann Meier P (2008) Phylogenetic distribution and membrane topology of the LytR-CpsA-Psr protein family. *BMC Genomics* **9:** 617

Hübscher J, McCallum N, Sifri CD, Majcherczyk PA, Entenza JM, Heusser R, Berger-Bachi B, Stutzmann Meier P (2009) MsrR contributes to cell surface characteristics and virulence in *Staphylococcus aureus*. *FEMS Microbiol Lett* **295:** 251–260

Ishikawa S, Kawai Y, Hiramatsu K, Kuwano M, Ogasawara N (2006) A new FtsZ-interacting protein, YlmF, complements the activity of FtsA during progression of cell division in *Bacillus subtilis*. *Mol Microbiol* **60:** 1364–1380

Jones LJ, Carballido-Lopez R, Errington J (2001) Control of cell shape in bacteria: helical, actin-like filaments in *Bacillus subtilis*. *Cell* **104:** 913–922

Kawai Y, Asai K, Errington J (2009a) Partial functional redundancy of MreB isoforms, MreB, Mbl and MreBH, in cell morphogenesis of *Bacillus subtilis*. *Mol Microbiol* **73:** 719–731

Kawai Y, Daniel RA, Errington J (2009b) Regulation of cell wall morphogenesis in *Bacillus subtilis* by recruitment of PBP1 to the MreB helix. *Mol Microbiol* **71:** 1131–1144

Kruse T, Bork-Jensen J, Gerdes K (2005) The morphogenetic MreBCD proteins of *Escherichia coli* form an essential membrane-bound complex. *Mol Microbiol* **55:** 78–89

Kuwana R, Kasahara Y, Fujibayashi M, Takamatsu H, Ogasawara N, Watabe K (2002) Proteomics characterization of novel spore proteins of *Bacillus subtilis*. *Microbiology* **148:** 3971–3982

Langer G, Cohen SX, Lamzin VS, Perrakis A (2008) Automated macromolecular model building for X-ray crystallography using ARP/wARP version 7. *Nat Protoc* **3:** 1171–1179

Lassila JK, Zalatan JG, Herschlag DL (2011) Biological phosphoryl-transfer reactions: understanding mechanism and catalysis. *Annu Rev Biochem* **80:** 669–702

Latge JP (2007) The cell wall: a carbohydrate armour for the fungal cell. *Mol Microbiol* **66:** 279–290

Lazarevic V, Karamata D (1995) The *tagGH* operon of *Bacillus subtilis* 168 encodes a two-component ABC transporter involved in the metabolism of two wall teichoic acids. *Mol Microbiol* **16:** 345–355

Lazarevic V, Margot P, Soldo B, Karamata D (1992) Sequencing and analysis of the *Bacillus subtilis lytRABC* divergon: a regulatory unit encompassing the structural genes of the N-acetylmuramoyl-L-alanine amidase and its modifier. *J Gen Microbiol* **138:** 1949–1961

Leaver M, Errington J (2005) Roles for MreC and MreD proteins in helical growth of the cylindrical cell wall in *Bacillus subtilis*. *Mol Microbiol* **57:** 1196–1209

Leslie AG (2006) The integration of macromolecular diffraction data. *Acta Crystallogr D Biol Crystallogr* **62:** 48–57

Massidda O, Kariyama R, Daneo-Moore L, Shockman GD (1996) Evidence that the PBP 5 synthesis repressor (*psr*) of *Enterococcus hirae* is also involved in the regulation of cell wall composition and other cell wall-related properties. *J Bacteriol* **178:** 5272–5278

McNeil M, Darvill AG, Fry SC, Albersheim P (1984) Structure and function of the primary cell walls of plants. *Annu Rev Biochem* **53:** 625–663

Morona JK, Morona R, Paton JC (2006) Attachment of capsular polysaccharide to the cell wall of *Streptococcus pneumoniae* type 2 is required for invasive disease. *Proc Natl Acad Sci USA* **103:** 8505–8510

Neuhaus FC, Baddiley J (2003) A continuum of anionic charge: structures and functions of D-alanyl-teichoic acids in gram-positive bacteria. *Microbiol Mol Biol Rev* **67:** 686–723

Pape T, Schneider TR (2004) HKL2MAP: a graphical user interface for phasing with SHELX programs. *J Appl Cryst* **37:** 843–844

Scheffers DJ, Jones LJ, Errington J (2004) Several distinct localization patterns for penicillin-binding proteins in *Bacillus subtilis*. *Mol Microbiol* **51:** 749–764

Schirner K, Errington J (2009) The cell wall regulator σI specifically suppresses the lethal phenotype of *mbl* mutants in *Bacillus subtilis*. *J Bacteriol* **191:** 1404–1413

Schirner K, Stone LK, Walker S (2011) ABC transporters required for export of wall teichoic acids do not discriminate between different main chain polymers. *ACS Chem Biol* **6:** 407–412

Sheldrick GM (2010) Experimental phasing with SHELXC/D/E: combining chain tracing with density modification. *Acta Crystallogr D Biol Crystallogr* **66:** 479–485

Slovak PM, Wadhams GH, Armitage JP (2005) Localization of MreB in *Rhodobacter sphaeroides* under conditions causing changes in cell shape and membrane structure. *J Bacteriol* **187:** 54–64

Soldo B, Lazarevic V, Karamata D (2002) *tagO* is involved in the synthesis of all anionic cell-wall polymers in *Bacillus subtilis* 168. *Microbiology* **148:** 2079–2087

Strahl H, Hamoen LW (2010) Membrane potential is important for bacterial cell division. *Proc Natl Acad Sci USA* **107:** 12281–12286

Swoboda JG, Campbell J, Meredith TC, Walker S (2010) Wall teichoic acid function, biosynthesis, and inhibition. *Chembiochem* **11:** 35–45

Swoboda JG, Meredith TC, Campbell J, Brown S, Suzuki T, Bollenbach T, Malhowski AJ, Kishony R, Gilmore MS, Walker S (2009) Discovery of a small molecule that blocks wall teichoic acid biosynthesis in *Staphylococcus aureus*. *ACS Chem Biol* **4:** 875–883

Tomasz A, McDonnell M, Westphal M, Zanati E (1975) Coordinated incorporation of nascent peptidoglycan and teichoic acid into pneumococcal cell walls and conservation of peptidoglycan during growth. *J Biol Chem* **250:** 337–341

Vats P, Shih YL, Rothfield L (2009) Assembly of the MreB-associated cytoskeletal ring of *Escherichia coli*. *Mol Microbiol* **72:** 170–182

Wei Y, Havasy T, McPherson DC, Popham DL (2003) Rod shape determination by the *Bacillus subtilis* class B penicillin-binding proteins encoded by *pbpA* and *pbpH*. *J Bacteriol* **185:** 4717–4726

Weidenmaier C, Peschel A (2008) Teichoic acids and related cell-wall glycopolymers in Gram-positive physiology and host interactions. *Nat Rev Microbiol* **6:** 276–287

Wolters PJ, Hildebrandt KM, Dickie JP, Anderson JS (1990) Polymer length of teichuronic acid released from cell walls of *Micrococcus luteus*. *J Bacteriol* **172:** 5154–5159

Wu LJ, Ishikawa S, Kawai Y, Oshima T, Ogasawara N, Errington J (2009) Noc protein binds to specific DNA sequences to coordinate cell division with chromosome segregation. *EMBO J* **28:** 1940–1952

Yokoyama K, Mizuguchi H, Araki Y, Kaya S, Ito E (1989) Biosynthesis of linkage units for teichoic acids in gram-positive bacteria: distribution of related enzymes and their specificities for UDP-sugars and lipid-linked intermediates. *J Bacteriol* **171:** 940–946

Young M, Mauel C, Margot P, Karamata D (1989) Pseudo-allelic relationship between non-homologous genes concerned with biosynthesis of polyglycerol phosphate and polyribitol phosphate teichoic acids in *Bacillus subtilis* strains 168 and W23. *Mol Microbiol* **3:** 1805–1812